View metadata, citation and similar papers at core.ac.uk

brought to you by CORE

provided by CiteSeerX

Peng Wang
School of Energy and Power Engineering,
University of Shanghai for Science
and Technology,
Shanghai 200093, China

Mo Yang[1]
School of Energy and Power Engineering,
University of Shanghai for Science
and Technology,
Shanghai 200093, China
e-mail: yangm@usst.edu.cn

Zhiyun Wang
School of Energy and Power Engineering,
University of Shanghai for Science
and Technology,
Shanghai 200093, China

Yuwen Zhang
Department of Mechanical
and Aerospace Engineering,
University of Missouri,
Columbia, MO 65211

A New Heat Transfer Correlation for Turbulent Flow of Air With Variable Properties in Noncircular Ducts

Turbulent flow and heat transfer of air with variable properties in a set of regular polygonal ducts and circular tube have been numerically simulated. All the ducts have the same hydraulic diameter as their characteristic lengths in the Reynolds number. The flow is modeled as three-dimensional (3D) and fully elliptic by using the finite volume method and the standard k-ε turbulence model. The results showed that the relatively strong secondary flow could be observed with variable properties fluid. For the regular polygonal ducts, the local heat transfer coefficient along circumferential direction is not uniform; there is an appreciable reduction in the corner region and the smaller the angle of the corner region, the more appreciable deterioration the corner region causes. The use of hydraulic diameter for regular polygonal ducts leads to unacceptably large errors in turbulent heat transfer determined from the circular tube correlations. Based on the simulation results, a correction factor is proposed to predict turbulent heat transfer in regular polygonal ducts. [DOI: 10.1115/1.4027855]

Keywords: variable properties, regular polygonal ducts, numerical simulation, secondary flow, correction factor

1 Introduction

Ducts with noncircular cross section are widely used in the heat exchangers and other devices. Prediction of the flow and heat transfer performances for noncircular ducts plays a key role on the design and manufacture of the engineering equipments. Developing and developed laminar flow and heat transfer in noncircular ducts have been extensively studied, and the results are well documented [1,2].

Turbulent forced-convection heat transfer in a noncircular duct is often encountered because of technical demands or design requirements. It has been a common practice to utilize the hydraulic diameter D_h as a characteristic length to obtain pressure drop and heat transfer coefficient in the noncircular ducts using correlations for circular tube. In other words, the hydraulic diameter D_h is recommended to be used in place of D in the Reynolds number, which is then applied to calculate f and Nu from the correlations for circular tube. The hydraulic diameter of noncircular duct provides a basis to approximate the friction factor and heat transfer coefficient for noncircular duct [3].

Nevertheless, it should be noted that for laminar fully developed heat transfer the Nusselt numbers difference between equilateral triangular duct and circular tube are 1.25 and 1.19 for uniform wall heat flux and uniform wall temperature, respectively, which are almost half of the Nusselt numbers for equilateral triangular duct (3.11 and 2.47) [2]. In addition, the use of hydraulic diameter for noncircular ducts such as triangular ducts leads to unacceptably large errors, in the order of 30%, in turbulent flow friction factors determined from the circular tube correlations [4–8]. A number of methods or characteristic lengths have been proposed to predict the pressure drop of turbulent flow in noncircular ducts [9–11].

Because of the analogy between the flow and heat transfer performances, it is questionable that whether the use of D_h in place of D to approximate heat transfer in noncircular duct is suitable or not.

To this problem, Lienhard [3] has pointed out that the results attained by substituting D_h for D in turbulent circular tube correlation are generally accurate to within ±20%, and worse results are obtained for duct cross-sections having sharp corners, such as an acute triangle. Although specialized equations for "effective" hydraulic diameters have been developed, it is only suitable for several kinds of specific geometries with the accuracies improved to 5–10% [12]. Using the square root of cross-sectional area as the dimensionless parameter, Duan [10] presented a new correlative model for fully developed turbulent flow and heat transfer in noncircular ducts. In the prediction of the friction factor, the new correlation model was in good agreement with the available experimental data. But the correlation for heat transfer was derived from hydrodynamic experiments instead of heat transfer experiments due to a shortage of enough reliable turbulent heat transfer experimental data in noncircular duct. To discern the problem and ameliorate the current correlative formula for noncircular ducts, more data and investigations are needed.

While a large number of investigations have been conducted on turbulent heat transfer performance in circular tube [13–17], experiments on the flow and heat transfer performances in noncircular ducts are limited because of the difficulty in the precise fabrication of noncircular ducts. In addition, it is difficult to deal with the unevenly distributed local wall temperature, as well as to measure the fluid bulk temperature and to diminish the measurement uncertainties. Meanwhile, a survey of the available literatures indicates that the experimental data on the pressure drop in the noncircular ducts, by contrast, are a bit more sufficient than that on the heat transfer for its relative easiness to measure and control. Jones [18] measured the frictional pressure drop in rectangular ducts, and proposed a *laminar equivalent* Reynolds number, which can make the circular tube methods readily applied to rectangular ducts. Hirota et al. [19] presented an experimental work on the turbulent heat transfer in a square duct. Eckert and Irvine [5] studied the pressure drop and heat transfer performance in a duct with an isosceles-triangular cross section. The experimental

[1]Corresponding author.

Contributed by the Heat Transfer Division of ASME for publication in the JOURNAL OF HEAT TRANSFER. Manuscript received May 2, 2013; final manuscript received June 5, 2014; published online July 2, 2014. Assoc. Editor: Ali Ebadian.

 Copyright © 2014 by ASME

Downloaded From: https://heattransfer.asmedigitalcollection.asme.org on 06/29/2019 Terms of Use: http://www.asme.org/about-asme/terms-of-use

results revealed that the heat transfer coefficients averaged over the circumference of the duct were half as large as values calculated from circular tube relations in the Reynolds number range from 4300 to 24,000. Malak et al. [20] studied the influence of several special channel geometries on pressure losses and heat transfer in noncircular channels with hydraulically smooth walls. Aly et al. [21] investigated the fully developed air-flows in an equilateral triangular duct over a Reynolds number range of 53,000–107,000.

With the development and improvement of the numerical simulation method, more and more investigations on the turbulent flow and heat transfer in noncircular ducts have been carried out by numerical simulations in conjunction with experiments. Emery et al. [22] simulated the developing turbulent flow and heat transfer characteristics in a square duct, and the simulation results were shown to be in good agreement with the measured data and the predictions using the k-ε closure model. Aolin et al.[23] applied the k-ε turbulence model in conjunction with the wall functions method to predict the developing flow and heat transfer performances in a triangular duct. Good agreement was found between the numerical simulation results and the measured data. Domaschke et al. [24] measured heat transfer and pressure drop in the channel of the internal cooling system of a gas turbine blade. In addition, they also carried out numerical simulations to analyze the flow and temperature fields in the channel. Nakayama et al. [25] analyzed the fully developed flow in ducts with rectangular and trapezoidal cross-sections by using a finite-difference method with the model of Launder and Ying [26]. Wang et al. [27] investigated the developing turbulent flow and heat transfer in a square duct based on the standard k-ε turbulence model, and good agreement between experimental and numerical results was obtained. Nguyen and Kazuhide [28] performed a numerical simulation with the k-ε turbulence model to investigate the behavior of airflow in the ventilation duct, and good agreement was found between the numerical results and the particle image velocimetry (PIV) measurement data. Yang and Ebadian [29] presented the numerical prediction of thermally developing flow in a square duct for turbulent flow with isothermal walls, and the computed results were shown to be in good agreement with the measured data.

In conclusion, experiments on turbulent flow characteristics in smooth and straight noncircular ducts have been conducted by some researchers in the early years. Most correction factors for the prediction of turbulent flow and heat transfer performances in noncircular ducts are appropriate for duct of a single or special geometry, and a general correction factor that can be applied to all cross-sectional shape is lacking. The discrepancies between results obtained from different researchers for the same geometry often exist and sometimes can be significant. Therefore, comparison of heat transfer results for different geometries obtained by different researchers becomes very challenge and obtaining a general correction factor through this approach is difficult. On the contrary, computational fluid dynamics (CFD) is a very effective method to ensure the differences between different geometries are caused by the geometries only and effects of any other uncertainties can be excluded.

The objective of the present work is to investigate the turbulent flow and heat transfer performances in a set of noncircular ducts. Heat transfer during turbulent air flow in the equilateral triangular, square, regular hexagonal, regular octagonal, regular dodecagonal ducts, and circular tube will be numerically simulated. All the ducts have the same hydraulic diameter D_h as their characteristic lengths in the Reynolds number. The flow and heat transfer performances for the above ducts will be compared.

2 Physical Model and Numerical Solution

2.1 Problem Description. Figure 1 shows the schematic diagram of the computational model, which is a simplified model of the experimental apparatus presented in Ref. [17]. As seen in Fig. 1, air flows through the calming section 1 before entering the heated duct zone. The dimensionless ratio L/D_h of calming section 1 is 61, which ensures that the fully developed flow is achieved at the entrance of the heated zone. Heat is transferred from the duct walls with uniform heat flux to the air inside it. The L/D_h of the heated zone is 60, and it is larger than the dimensionless thermal entry length. In the experiment conducted by Babas' Haq [17], the calming section 2 was employed to eliminate the deviations caused by the "end effects" which is the result of the sudden change at the outlet. Here it is appended to improve the accuracy of simulation by making the outlet farther from the heated duct zone [30].

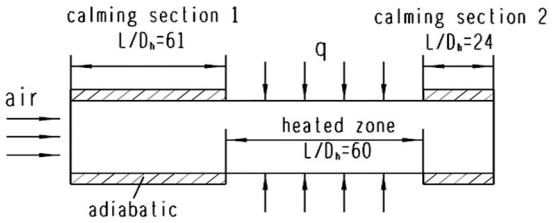

Fig. 1 Schematic diagram of the computational model

2.2 Governing Equations. In this work, air with variable properties is used as the working fluid to study the flow and heat transfer performances for the ducts shown in Fig. 1. The properties that are variable contain density ρ, heat capacity c_p, thermal conductivity λ, and dynamic viscosity μ.

Selection of appropriate turbulence model is very important to correctly and effectively study the flow and heat transfer characteristics in the ducts. Albets-Chico et al. [31] applied several turbulence models to the duct flow, including the k-ε model combined with wall-function treatment [32], as well as the Ince–Launder low Reynolds number k-ε model [33] and the Wilcox k-ω turbulence model [34]. After comparing the numerical results with the direct numerical simulation (DNS) data [35] and experimental results, the k-ε model in conjunction with wall function methods were proved to be a good choice to conduct the investigation in this work due to its low central processing unit (CPU) consumption and appreciate accuracy. Moreover, the works by Aolin et al. [23] and Wang et al. [27] are also in favor of the application of the standard k-ε model [36].

The time-averaged governing equations of the fluid flow will be given based on the following assumptions: the fluid is Newtonian, the properties are variable but only in accordance with the temperature, nonparticipant radiant medium, and the body forces are negligible. Additionally, it is assumed that the time averaged values are constant in time, so the turbulence is deemed to be steady. The governing equations in tensorial form are shown as follows:

$$\frac{\partial\left(\rho\overline{u_j}\right)}{\partial x_j}=0 \tag{1}$$

$$\frac{\partial\left(\rho\overline{u_i}\overline{u_j}\right)}{\partial x_j}=-\frac{\partial\overline{P}}{\partial x_i}+\frac{\partial}{\partial x_j}\left[\mu\left(\frac{\partial\overline{u_i}}{\partial x_j}+\frac{\partial\overline{u_j}}{\partial x_i}-\frac{2}{3}\delta_{i,j}\frac{\partial\overline{u_i}}{\partial x_i}\right)\right]+\frac{\partial}{\partial x_j}\left(-\rho\overline{u_i'u_j'}\right) \tag{2}$$

$$\frac{\partial\left(\rho c_p\overline{u_i}\overline{T}\right)}{\partial x_i}=\frac{\partial}{\partial x_i}\left(\lambda\frac{\partial\overline{T}}{\partial x_i}\right)+\frac{\partial}{\partial x_i}\left(-\rho c_p\overline{u_i'T'}\right) \tag{3}$$

$$\frac{\partial\left(\rho\overline{u_j}k\right)}{\partial x_j}=\frac{\partial}{\partial x_j}\left[\left(\mu+\frac{\mu_t}{\sigma_k}\right)\frac{\partial k}{\partial x_j}\right]+G_k-\rho\varepsilon \tag{4}$$

$$\frac{\partial\left(\rho\overline{u_j}\varepsilon\right)}{\partial x_j}=\frac{\partial}{\partial x_j}\left[\left(\mu+\frac{\mu_t}{\sigma_\varepsilon}\right)\frac{\partial\varepsilon}{\partial x_j}\right]+\frac{C_1\varepsilon}{k}G_k-C_2\rho\frac{\varepsilon^2}{k} \tag{5}$$

$$\mu_t=\frac{C_\mu\rho k^2}{\varepsilon} \tag{6}$$

Downloaded From: https://heattransfer.asmedigitalcollection.asme.org on 06/29/2019 Terms of Use: http://www.asme.org/about-asme/terms-of-use

Table 1 Average Nusselt number for different mesh sizes at cross section

Mesh size	343 × 435	505 × 435	1122 × 435	1651 × 435	2581 × 435
Nu	116.57	112.36	110.55	110.43	110.68

Table 2 Average Nusselt number for different mesh sizes in the direction of the flow

Mesh size	1122 × 218	1122 × 310	1122 × 435	1122 × 870
Nu	113.86	111.57	110.55	110.32

where

$$-\rho\overline{u_i'u_j'} = -\frac{2}{3}\rho k\delta_{i,j} + \mu_t\left(\frac{\partial\overline{u_i}}{\partial x_j} + \frac{\partial\overline{u_j}}{\partial x_i}\right) - \frac{2}{3}\mu_t\delta_{i,j}\frac{\partial\overline{u_k}}{\partial x_k} \quad (7)$$

$$-\rho\overline{u_j'T'} = \frac{\mu_t}{\sigma_T}\frac{\partial\overline{T}}{\partial x_j} \quad (8)$$

$$G_k = -\rho\overline{u_i'u_j'}\frac{\partial\overline{u_i}}{\partial x_j} \quad (9)$$

The values of the coefficients shown above were adopted from Refs. 36–38, i.e., $C_\mu = 0.09$; $C_1 = 1.44$; $C_2 = 1.92$; $\sigma_k = 1.0$; $\sigma_\varepsilon = 1.3$; $\sigma_T = 0.85$.

2.3 Boundary Conditions. The outlet boundary condition of the computational domain is treated by local one-way method [30]. At the walls, the velocity is set to be zero and the heat flux q is given as a constant. The boundary condition for k imposed at the wall is $(\partial k/\partial n)_w = 0$. At the wall-adjacent cells the ε equation is not solved and ε is computed by employing the equation, $\varepsilon_p = \left(C_\mu^{3/4}k_p^{3/2}\right)/(\kappa y_p)$. Uniform velocity and kinetic energy of turbulence are assumed at the duct inlet. For the energy equation the wall functions are used to determine the wall temperature from the calculated near wall temperature fields, as the heat flux is prescribed at the wall. The difference between the wall temperature and the local bulk temperature is then used to calculate the local heat transfer coefficient.

2.4 Numerical Approach. The numerical simulations are performed by solving fully elliptic 3D Navier–Stokes equations. The numerical investigation is conducted using commercial solver FLUENT which employs the finite volume method [39] to discretize the governing equations. In this procedure the computational domain is discretized by a series of control volumes, and the governing equations are then integrated over a control volume. The QUICK-type scheme is adopted to discretize the convection terms. The pressure–velocity coupling is handled by the SIMPLE algorithm [30]. The computational time for one case is approximate 2 h using a computer with Intel Core i5 (3.20 GHz). Extensive comparisons between the simulation results and the available experimental data will be presented to show the credibility and reliability of the numerical approach.

2.5 Data Reduction. The local bulk temperature is calculated by

$$T_{b,x} = \frac{\int_0^{A_{c,x}} \rho u c_p T dA_{c,x}}{\int_0^{A_{c,x}} \rho u c_p dA_{c,x}} \quad (10)$$

where $A_{c,x}$ is the area of the cross section at the axial position of x.

The local wall temperature is obtained from

$$T_{w,x} = \frac{1}{A_{w,x}}\int_0^{A_{w,x}} T_{w,x,i} dA_{w,x} \quad (11)$$

where $A_{w,x}$ is the surface area of the wall with axial position x, and $T_{w,x,i}$ is the wall temperature that can be different at different circumferential locations.

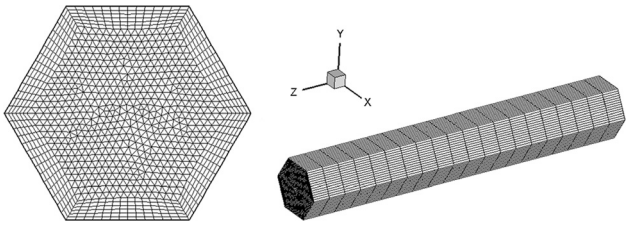

Fig. 2 Sample of computational mesh (not in scale)

The local heat transfer coefficient is calculated by

$$h_x = q/(T_{w,x} - T_{b,x}) \quad (12)$$

where q is the wall heat flux, which is assumed to be constant in this work.

The duct average Nusselt number and Reynolds number are

$$\mathrm{Nu} = qD_h/[\lambda(T_w - T_b)], \quad \mathrm{Re} = \rho u D_h/\mu = \rho_{in}u_{in}D_h/\mu \quad (13)$$

The characteristic length, average bulk temperature, friction factor, and average wall temperature of the duct are defined by

$$D_h = 4A_c/p, \quad T_b = (T_{b,in} + T_{b,out})/2$$
$$T_w = \frac{1}{A}\int_0^A T_{w,x}dA, \quad f = 2\frac{\Delta p}{\rho u^2}\frac{D_h}{L} \quad (14)$$

where A_c is the cross-sectional area, p is the wetted perimeter of the duct, and A is the surface area of the heated zone of the duct.

In this investigation, T_b is taken as the reference temperature to evaluate the properties of the fluid.

2.6 Grid Independence. The grid independence of the numerical result is studied for all the six ducts. Take the regular hexagonal duct for example, under the premise of ensuring the value of y^+ for the first inner node accord with the requirement of the wall functions, i.e., $y^+ > 15$, Tables 1 and 2 list the variations of the Nusselt number along with the mesh size at the Reynolds number of 53,477. The mesh size is given in the form of $A \times B$, where A stands for the number of nodes at any cross section, B stands for the number of nodes in the direction of the flow. It can be seen that the mesh size 1122×435 is sufficient to obtain grid independent solution for the case. Figure 2 shows the grid system for the regular hexagonal duct.

3 Results and Discussion

3.1 Circular Tube. The average Nusselt number and local heat transfer coefficients for turbulent air flow in a circular tube are shown in Figs. 3 and 4, respectively.

It can be seen that the maximum deviations between the current numerical results and the Nusselt number predicted by the correlations of Dittus–Boelter [13], McAdams [14], and Gnielinski [16] are 9.7%, 7.1%, and 3.9%, respectively. The agreement between the numerical results and those of previous investigations is generally satisfactory. The average Nusselt number predicted by the Dittus–Boelter [13] correlation is higher than that obtained by the current simulation. This agrees with the experimental correlations of McAdams [14] and Babas' Haq [17], and the formulations of

Downloaded From: https://heattransfer.asmedigitalcollection.asme.org on 06/29/2019 Terms of Use: http://www.asme.org/about-asme/terms-of-use

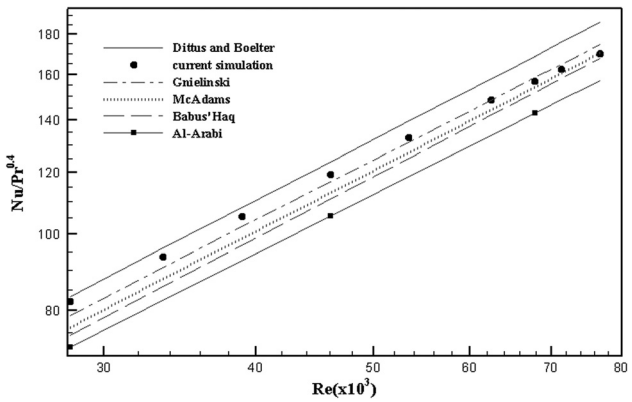

Fig. 3 Comparison between the numerical results and those of previous investigations

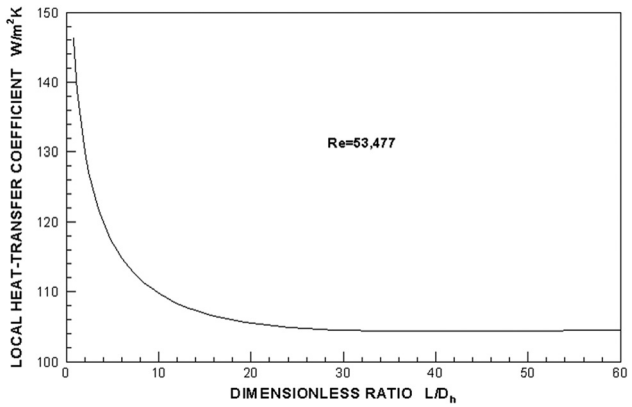

Fig. 4 Variation of the local heat transfer coefficient versus the dimensionless ratio L/D_h

Gnielinski [16]. In addition, the friction factors for the circular tube under the nine cases were compared with the prediction by Blasius equation [40] and Filonenko formula [41], and the differences are less than 6.4%.

Figure 4 shows the variation of the local heat transfer coefficient h_x along the axial direction of the circular tube (the heated zone in Fig. 1) at the Reynolds number of 53,477. The local heat transfer coefficient decreases gradually until a limit is reached at the thermal entry length. In the case shown in Fig. 4 the *thermal entry length*, which is defined as the length of the tube required to achieve a local value of h_x equal to 1.05 times the asymptotic values of the corresponding h_∞ for a certain thermal boundary condition specified at the surface [42], is approximately $L/D_h = 11.5$; it is almost the same position as that attained by Babas' Haq [17] who conducted the experiment with the circular tube shown in Fig. 1. In addition, the numerical simulation results indicate the same conclusion as Babas' Haq's experiment, that is, the thermal entry length is not strongly sensitively to the magnitude of Reynolds number.

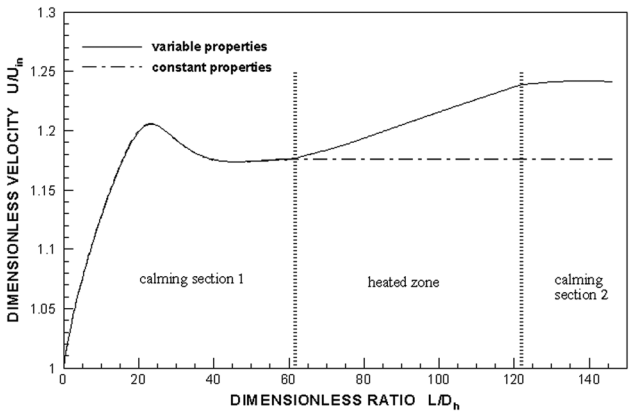

Fig. 5 Variation of the dimensionless axial velocity along the circular tube

3.2 Regular Polygonal Ducts. Turbulent air flow in the equilateral triangular, square, regular hexagonal, regular octagonal and regular dodecagonal ducts are simulated. All the regular polygonal ducts have the same structure shown in Fig. 1 and the same hydraulic diameter D_h. In order to simplify the presentation, symbols that are adopted for the six ducts are summarized in Table 3. The "axial velocity" in the text refers in particular to the axial velocity on the axis of the ducts. For a concise presentation, the flow and heat-transfer characteristics for the regular polygonal ducts and a circular tube with diameter equal to D_h will also be provided.

3.2.1 Flow Characteristics. Figure 5 shows the variation of the dimensionless axial velocity along the axial direction of the circular tube (including calming section 1, heated zone and calming section 2). Comparing the variation of the axial velocity for variable properties fluid with that for constant properties fluid, the following features may be noted. First, in the calming section 1, the two cases have almost the same trend because the calming section 1 does not exchange heat with the air inside it, and hence there is no change in the properties. There is a maximum value, which is called the "crest value" for the axial velocity. The crest value is the result of the boundary layer, secondary flow, and stochastic motion caused by the turbulence. Second, in the heated zone, the axial velocity is constant for the constant properties fluid, but increases gradually for the variable properties fluid since the air density decreases with increasing temperature. In the calming section 2, both the axial velocities of the two fluids are constants because there is no heat transferred from the duct wall to the fluid and no change in the properties.

Figure 6 shows the patterns of the secondary flow at different axial positions in the regular hexagonal duct for the variable properties fluid under a Reynolds number of 53,477. Additionally, the patterns of the secondary flow for the constant properties fluid are shown in Fig. 7. It can be seen that when compare with the mean axial velocity, the secondary flow are very weak for all cross sections. However, at the hydrodynamic entrance zone, both working fluids have relatively strong secondary flows

Table 3 Regular polygonal ducts

Geometry	Circle	Equilateral triangle	Square	Regular hexagon	Regular octagon	Regular dodecagon
Symbol	A-1	A-3	A-4	A-6	A-8	A-12
Shape	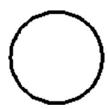		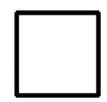	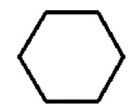	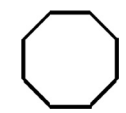	

Downloaded From: https://heattransfer.asmedigitalcollection.asme.org on 06/29/2019 Terms of Use: http://www.asme.org/about-asme/terms-of-use

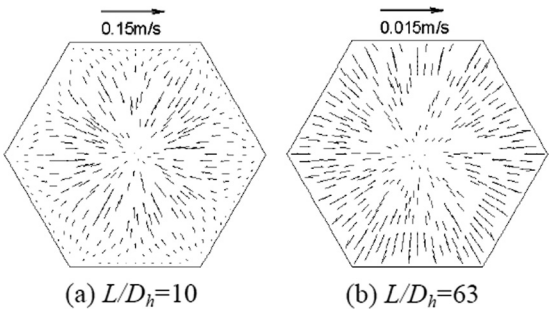

Fig. 6 Regular hexagonal cross section velocity filed for variable properties fluid

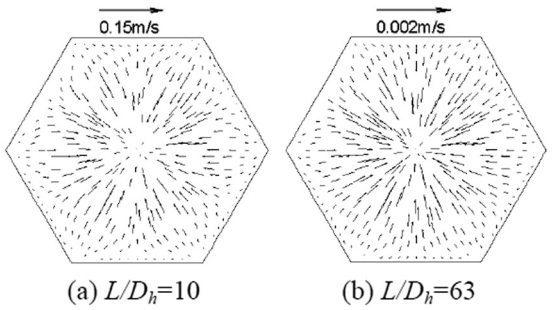

Fig. 7 Regular hexagonal cross section velocity filed for constant properties fluid

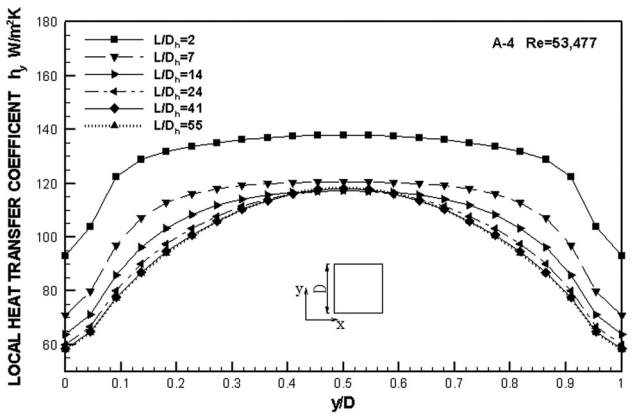

Fig. 8 Distributions of the circumferential local heat transfer coefficient h_y in the heated zone of the square duct

(see Figs. 6(*a*) and 7(*a*)). This is caused by the wall damping effect, which slows down the velocity field of the fluid near the wall and compels the fluid to move from the outside to the inner core of the cross section. After a certain distance, the secondary flow turns to be too weak to be observed. From Figs. 6(*b*) and 7(*b*), it can be observed that in the heated zone, the secondary flow for the variable properties fluid is stronger than that for the constant properties fluid and the magnitude of the secondary flow is relatively strong near the wall. This is basically because the temperature of the fluid increases as heat is transferred from the duct to the fluid, and for the variable properties fluid, higher temperature leads to lower density ρ and higher viscosity μ. Although the velocity of the near-wall fluid should increase to conserve the mass flux in principle, some fluid moves from the near-wall region to the inner core of the duct because of the presence of the wall, and hence stronger secondary flow can be observed for variable

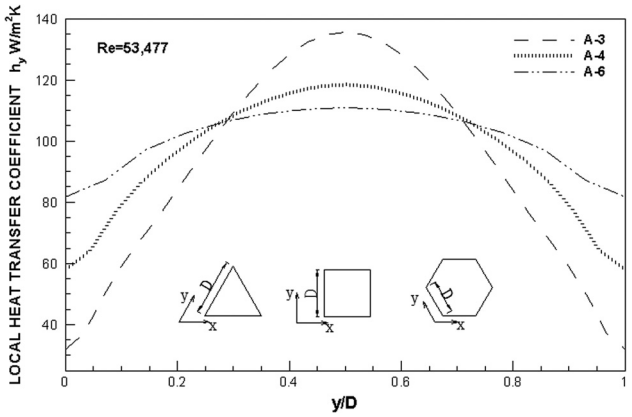

Fig. 9 Distributions of the circumferential local heat transfer coefficient h_y for fully developed heat transfer of the ducts A-3, A-4, and A-6

properties fluid. In fact, for the constant properties fluid there is nearly no change in the patterns of the secondary flow in the heated zone, for the independence between the properties and the temperature. The patterns of the secondary flow for the constant properties fluid in the square duct is almost the same with that reported by Wang et al. [27]. The above can also give the explanation to the increase of the axial velocity in the heated zone (see Fig. 5).

3.2.2 Local Heat-Transfer Characteristics. Figure 8 shows the distributions of the circumferential local heat transfer coefficient along the axial direction in the heated zone of the square duct. It can be seen that compared with the other parts of the wall, the heat transfer coefficient is relatively low in the duct corner. This is mainly caused by the blocking effect of the corner walls which appreciably slows down the fluid velocity in the corner regions, thereby deteriorates the local heat transfer. The distribution characteristic is similar to the measurement results from Wang et al. [27] and the prediction by Fleming and Sparrow [43] and Aolin et al. [23]. Comparing the distributions of the circumferential local heat transfer coefficient at $L/D_h = 2$ with $L/D_h = 7$, the heat transfer coefficient decreases appreciably in the thermal entrance region. When we make a comparison between the distributions at $L/D_h = 41$ and $L/D_h = 55$, it is easy to find that along the axial position of the duct, the local heat transfer coefficient h_x reduces to a constant. The shapes of the circumferential local heat transfer coefficient distribution curves illustrate that along the axial position, the part of the wall that is influenced by the corner's blocking effect enlarges gradually.

Figure 9 illustrates the distributions of the circumferential local heat transfer coefficient of the ducts A-3, A-4, and A-6 for fully developed turbulent heat transfer. It presents that the corner region deteriorates the local heat transfer appreciably. And the extent of the influence on the heat transfer characteristic is related to the angle of the corner region, that is, the smaller the angle of the corner region, the more appreciable deterioration the corner region causes. Besides this, it can be seen that the maldistribution characteristic of the circumferential local heat transfer coefficient becomes more apparent as the angle of the corner region gets smaller.

3.3 Comparison of Heat Transfer Performances for all the Ducts. The values of the average Nusselt number for all the above ducts are summarized in Table 4. The numerical simulation covers a range of Reynolds number from 28,000 to 77,000.

For the regular polygonal ducts, a survey of available literature indicates that a large number of experimental investigations have been conducted on the noncircular ducts which are appended with ribs, fins, vortex generators, or roughed walls.

Downloaded From: https://heattransfer.asmedigitalcollection.asme.org on 06/29/2019 Terms of Use: http://www.asme.org/about-asme/terms-of-use

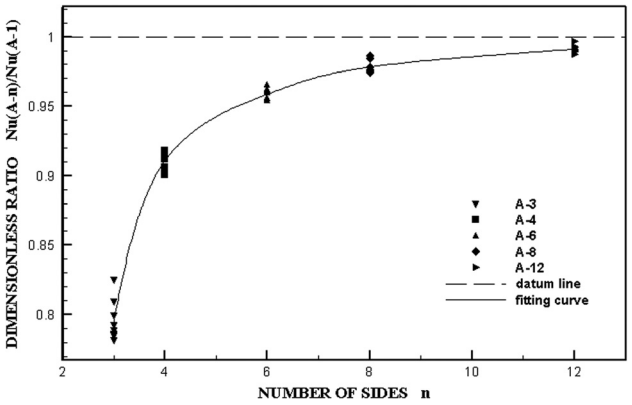

Fig. 10 The proportion of the average Nusselt number for regular polygonal duct on that for circular tube $Nu_{(A-n)}/Nu_{(A-1)}$ versus the number of sides of the ducts

Table 4 Values of the average Nusselt number for all the above ducts obtained by the current numerical simulation

Re \ Nu	A-1	A-3	A-4	A-6	A-8	A-12
28,119	70.99	58.58	64.82	68.52	70.01	70.51
33,576	81.35	65.86	74.18	78.05	79.53	81.07
38,985	91.14	72.85	82.10	86.95	88.86	90.41
46,085	103.22	81.78	93.00	99.29	101.6	102.19
53,477	114.99	90.66	104.18	110.55	112.45	113.90
62,507	128.37	100.91	117.16	123.36	125.55	126.96
67,895	135.84	106.23	124.28	129.86	132.31	134.48
71,468	140.52	110.33	128.76	134.06	137.01	139.26
76,828	147.19	115.66	135.16	140.56	143.66	145.27

However, the experiments on the turbulent flow and heat transfer in the smooth and straight long ducts are scant. It should also be noted that the experimental data on the turbulent heat transfer characteristics in noncircular ducts are much fewer than that on the turbulent flow characteristics. Non-negligible differences and sometimes even contradictions exist when compared with the measurement results of different authors on the channels of the same geometry. Nevertheless, it is encouraging that high consistence can be found among the experimental data of turbulent flow characteristics (include friction factor f) provided by different researchers.

The numerical results of the friction factor in equilateral triangular duct were compared with the measured data provided by Aly et al. [21], Schiller [44], and Nikuradse [45], and the maximum deviation is less than 4.3%. The differences between the numerical results for square duct with the experimental data from Schiller [44] are within 2.3%. Additionally, the comparisons of the friction factors for the other three regular polygonal ducts were also made between the numerical results and the predictions by Duan [10] and good agreements are found.

On the basis of the good agreement between the simulation results and the available experimental data, and the analogy between the flow and heat transfer performances, it can be concluded that the numerical approach applied to this investigation can make good performance on the prediction of the heat transfer characteristics in the ducts.

Figure 10 and Table 4 show that the difference between the average Nusselt numbers for the regular polygonal ducts and circular tube increases with the decreasing number of sides of the regular polygon. That is to say, the use of hydraulic diameter for noncircular ducts such as equilateral triangular duct will result in unacceptably large errors, on the order of 27.5%, in turbulent heat transfer Nusselt number determined from the circular tube correlations.

Table 5 Circularity C_ϕ of all the above ducts

Duct	A-1	A-3	A-4	A-6	A-8	A-12
C_ϕ	1	0.778	0.886	0.952	0.974	0.988

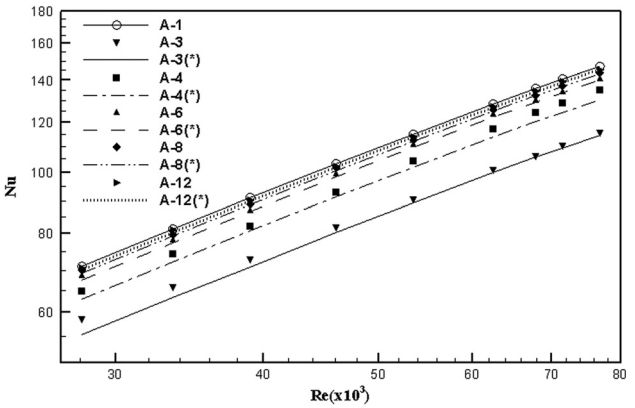

Fig. 11 Comparison between the numerical results and the new correlation Eq. (16)

In order to correct the large errors indicated above but also maintain the simple form of the existing correlations, a correction factor C_ϕ named circularity is proposed. It is defined to measure the degree of the closeness between the 2D graph and the circle

$$C_\phi = \pi d/p \tag{15}$$

where p is the perimeter of the 2D graph, d is the diameter of the circle that has the same area as the 2D graph.

Based on Eq. (15), the circularity C_ϕ of all the above ducts are summarized in Table 5.

Then, a new correlation in conjunction with C_ϕ is proposed as follows:

$$\mathrm{Nu} = C_\phi \cdot \mathrm{Nu}_{\mathrm{circle}} \tag{16}$$

where $\mathrm{Nu}_{\mathrm{circle}}$ is in place of the existing correlations, e.g., the correlations of Gnielinski [16] and Dittus–Boelter [13], the experimental correlations of McAdams [14], etc.

The current simulation results shown in Table 4 are illustrated in Fig. 11 in the form of scatter points, and the lines are obtained from Eq. (16) (the simulation results for circular tube take the place of $\mathrm{Nu}_{\mathrm{circle}}$ in Eq. (16)). It can be seen that there is a quite satisfactory agreement between them. In fact, for the equilateral triangular duct, the largest deviation between the results of numerical simulation and the new correlation Eq. (16) is 5.7%, and 3.5%, 1.4%, 1.3%, and 0.8% for the square, regular hexagonal, regular octagonal, and regular dodecagonal ducts, respectively.

4 Conclusions

A numerical study of turbulent forced-convection heat transfer in a set of noncircular ducts is presented in this paper. Air with variable properties is used as the working fluid in the numerical simulation, and the cross sections of the ducts are equilateral triangular, square, regular hexagonal, regular octagonal, regular dodecagonal and circular. All the ducts have the same hydraulic diameter as characteristic length in the Reynolds number. In the numerical study, the flow is modeled as 3D and fully elliptic by using finite volume method with uniform wall heat flux. The widely used k-ε turbulence model in conjunction with the wall functions method is adopted. The flow and heat transfer

Downloaded From: https://heattransfer.asmedigitalcollection.asme.org on 06/29/2019 Terms of Use: http://www.asme.org/about-asme/terms-of-use

performances for the above ducts are compared and the following conclusions can be drawn:

(1) For circular tube, the numerical results agree well with the previous experimental correlations.
(2) Stronger secondary flow can be observed for variable properties fluid than that for constant properties fluid.
(3) For the regular polygonal ducts, the heat transfer coefficient in the duct corner region is appreciably lower than that in the other part of the wall, and the smaller the angle of the corner region, the more appreciable deterioration the corner region causes.
(4) The use of hydraulic diameter for regular polygonal ducts such as equilateral triangular duct leads to unacceptably large errors, in the order of 27.5%, in turbulent flow heat transfer determined from the circular tube correlations.
(5) A circularity C_ϕ is proposed to correct the existing correlations, and it is to be noted that the deviations between the numerical simulation results and the new heat transfer correlation are within 6%.

However, it should be pointed out that the new correlation is only appropriate for the regular polygonal ducts, and more investigations are needed to modify the current correlations to apply to more noncircular ducts.

Acknowledgment

This work was supported by the National Natural Science Foundation of China (Grant Nos. 51276118, 51129602), Shanghai Science and Technology Innovation Action Plan of Shanghai Municipal Science and Technology Commission (Grant No. 12DZ1200100) and Public welfare scientific research projects of Shanghai Municipal Bureau of Quality and Technical Supervision (Grant No. 2012-41). The present authors would gratefully acknowledge the valuable advice from the referees.

Nomenclature

A = area (m^2)
c_p = heat capacity (J/(kg·K))
C_ϕ = correction factor circularity
D = diameter of the circular tube (m)
D_h = hydraulic diameter of the noncircular duct (m)
k = turbulent kinetic energy (m^2/s^2)
L= duct length (m)
Nu = Nusselt number
p = wetted perimeter (m)
P = pressure (Pa)
Pr = Prandtl number
q = heat flux (W/m^2)
Re = Reynolds number
T = temperature (K)
u = velocity (m/s)
x = coordinate (m)

Greek Symbols

δ_{ij} = Kronecker delta
ε = turbulent dissipation rate (m^2/s^3)
κ = von Karman constant (=0.42)
λ = thermal conductivity (W/(m·K))
μ = dynamic viscosity (kg/(m·s))
μ_t = eddy or turbulent viscosity (kg/(m·s))
ρ = density (kg/m^3)
σ_k = turbulent kinetic energy Prandtl number
σ_ε = turbulent dissipation rate Prandtl number
σ_T = turbulent energy Prandtl number

Subscripts

b = bulk
c = cross section
circle = circular tube
i = partial element
in = inlet
out = outlet
p = the first near-wall node
t = turbulence
w = wall
x = axial position of the duct
∞ = infinite length

Superscripts

$'$ = fluctuation value
$^-$ = time-averaged value

References

[1] Shah, R. K., and London, A. L., 1978, "Laminar Forced Convection in Ducts," *Advances in Heat Transfer: Supplement*, Academic, San Diego, CA.
[2] Yang, S. M., and Tao, W. Q., 2006, *Heat Transfer*, 4th ed., Higher Education, Beijing, China.
[3] Lienhard, J. H., 2006, *A Heat Transfer Textbook*, 3rd ed., Phlogiston, Cambridge, MA.
[4] Eckert, E. R. G., and Irvine, T. F., 1956, "Flow in Corners of Passages With Non-Circular Cross Sections," Trans. ASME, **78**(4), pp. 709–718.
[5] Eckert, E. R. G., and Irvine, T. F., 1960, "Pressure Drop and Heat Transfer in a Duct With Triangular Cross-Section," ASME J. Heat Transfer, **82**(2), pp. 125–138.
[6] Carlson, L. W., and Irvine, T. F., 1961, "Fully Developed Pressure Drop in Triangular Shaped Ducts," ASME J. Heat Transfer, **83**(4), pp. 441–444.
[7] Nan, S. F., and Dou, M., 2000, "A Method of Correlating Fully Developed Turbulent Friction in Triangular Ducts," ASME J. Fluids Eng., **122**(3), pp. 634–636.
[8] Leung, C. W., Chan, T. L., and Chen, S., 2001, "Forced Convection and Friction in Triangular Duct With Uniformly Spaced Square Ribs on Inner Surfaces," Heat Mass Transfer, **3**, pp. 719–725.
[9] He, S., and Gotts, J. A., 2004, "Calculation of Friction Coefficients for Noncircular Channels," ASME J. Fluids Eng., **126**(6), pp. 1033–1038.
[10] Duan, Z. P., 2012, "New Correlative Models for Fully Developed Turbulent Heat and Mass Transfer in Circular and Noncircular Ducts," ASME J. Heat Transfer, **134**(1), p. 014503.
[11] Duan, Z. P., and Muzychka, Y. S., 2010, "Slip Flow in the Hydrodynamic Entrance Region of Circular and Noncircular Microchannels," ASME J. Fluids Eng., **132**(1), p. 011201.
[12] Bhatti, M. S., and Shah, R. K., 1987, "Turbulent and Transition Flow Convective Heat Transfer in Ducts," *Handbook of Single-Phase Convective Heat Transfer*, S. KaKac, R. K. Shah, and W. Aung, eds., Wiley, New York, Chap. 4.
[13] Dittus, F. W., and Boelter, L. M. K., 1930, *Heat Transfer in Automobile Radiators of the Tubular Type*, Vol. 2, University of California (Berkeley) Publications, Berkeley, CA, pp. 443–461.
[14] McAdams, W. H., 1954, *Heat Transmission*, McGraw-Hill, New York.
[15] AI-Arabi, M., 1958, "Study of Existing Data for Heating of Air and Water in Turbulent Flow in Inside Tubes," ASME Paper No. 58-A-298.
[16] Gnielinski, V., 1976, "New Equations for Heat and Mass Transfer in Turbulent Pipe and Channel Flow," Int. Chem. Eng., **16**, pp. 359–368.
[17] Babas' Haq, R. F., 1992, "Forced Convection Heat Transfer From a Pipe to Air Flowing Turbulently Inside It," Exp. Heat Transfer, **5**, pp. 161–173.
[18] Jones, D. C., 1976, "An Improvement in the Calculation of Turbulent Friction in Rectangular Ducts," ASME J. Fluids Eng., **98**(2), pp. 173–181.
[19] Hirota, M., Fujita, H., Yokosawa, H., Nakai, H., and Itoh, H., 1997, "Turbulent Heat Transfer in a Square Duct," Int. J. Heat Fluid Flow, **18**, pp. 170–180.
[20] Malak, J., Hejna, J., and Schmid, J., 1975, "Pressure Losses and Heat Transfer in Noncircular Channels With Hydraulically Smooth Walls," Int. J. Heat Mass Transfer, **18**, pp. 139–149.
[21] Aly, A. M. M., Trupp, A. C., and Gerrard, A. D., 1978, "Measurements and Prediction of Fully Developed Turbulent Flow in an Equilateral Triangular Duct," J. Fluid Mech., **85**, pp. 57–83.
[22] Emery, A. F., Neighbors, P. K., and Gessner, F. B., 1980, "The Numerical Prediction of Developing Turbulent Flow and Heat Transfer in a Square Duct," ASME J. Heat Transfer, **102**(1), pp. 51–57.
[23] Aolin, Ge, J. X., and Cai, Z. H., 1989, "An Investigation of Developing Flow and Heat Transfer in a Triangular Duct," J. Shanghai Inst. Mech. Eng. **11**(4), pp. 1–12.
[24] Domaschke, N., Wolfersdorf, J. V., and Semmler, K., 2012, "Heat Transfer and Pressure Drop Measurements in a Rib Roughened Leading Edge Cooling Channel," ASME J. Turbomach., **134**(6), p. 061006.
[25] Nakayama, A., Chow, W. L., and Sharma, D., 1983, "Calculation of Fully Development Turbulent Flows in Ducts of Arbitrary Cross Section," J. Fluid Mech., **128**, pp. 199–217.
[26] Launder, B. E., and Ying, W. M., 1973, "Prediction of Flow and Heat Transfer in Ducts of Square Cross Section," Proc. Inst. Mech. Eng., **187**, pp. 455–461.
[27] Wang, L. B., Wang, Q. W., He, Y. L., and Tao, W. Q., 2002, "Experimental and Numerical Study of Developing Turbulent Flow and

Downloaded From: https://heattransfer.asmedigitalcollection.asme.org on 06/29/2019 Terms of Use: http://www.asme.org/about-asme/terms-of-use

Heat Transfer in Convergent/Divergent Square Ducts," Heat Mass Transfer, **38**, pp. 399–408.
[28] Nguyen, L. P., and Kazuhide, I., 2013, "Experimental and Numerical Study of Airflow Pattern and Particle Dispersion in a Vertical Ventilation Duct," Build. Environ., **59**, pp. 466–481.
[29] Yang, G., and Ebadian, M. A., 1991, "Effect of Reynolds and Prandtl Numbers on Turbulent Convective Heat Transfer in a Three-dimensional Square Duct," Numer. Heat Transfer A, **20**, pp. 111–122.
[30] Patankar, S. V., 1980, *Numerical Heat Transfer and Fluid Flow*, Hemisphere Publishing Co., New York.
[31] Albets-Chico, X., Perez-Segarra, C. D., Oliva, A., and Bredberg, J., 2008, "Analysis of Wall-Function Approaches Using Two-Equation Turbulence Models," Int. J. Heat Mass Transfer, **51**, pp. 4940–4957.
[32] Launder, B. E., 1988, "On the Computation Convective Heat Transfer in Complex Turbulent Flows," ASME J. Heat Transfer, **110**(4b), pp. 1112–1128.
[33] Ince, N., and Launder, B. E., 1989, "Computation of Buoyancy-Driven Turbulent Flows in Rectangular Enclosures," Int. J. Heat Fluid Flow, **10**, pp. 110–117.
[34] Wilcox, D. C., 1994, "Simulation of Transition With a Two-Equation Turbulence Model," AIAA J., **32**, pp. 247–255.
[35] Moser, R. D., Kim, J., and Mansour, N. N., 1999, "Direct Numerical Simulation of Turbulent Chanel Flow Up to $Re_\tau = 590$," Phys. Fluids, **11**, pp. 943–945.
[36] Lauder, B. E., and Spalding, D. B., 1974, "The Numerical Computation of Turbulent Flows," Comput. Methods Appl. Mech. Eng., **3**, pp. 269–289.
[37] Markatos, N. C., 1986, "The Mathematical Modeling of Turbulence Flows," Appl. Math. Modell., **10**, pp. 190–220.
[38] Pourahmadi, F., and Humphery, J. A. C., 1983, "Prediction of Curved Channel Flow With an Extended k-ε Model of Turbulence," AIAA J., **21**, pp. 1365–1373.
[39] Tao, W. Q., 2001, *Numerical Heat Transfer*, Xi'an Jiaotong University, Xi'an, China.
[40] Blasius, H., 1913, "Das Ahnlichkeitsgesetz bei Reibungsvorgangen in Flussigkeiten," VDI Forschungsh., **131**, pp. 1–12.
[41] Filonenko, G. K., 1954, "Hydraulic Resistance in Pipes," Teploenergetika, **1**, pp. 40–44.
[42] Salazar, A. J., and Campo, A., 1990, "Prediction of the Thermal Entry Length Without Solving the Complete Entrance Length Problem," Int. J. Heat Fluid Flow, **11**(1), pp. 48–53.
[43] Fleming, D. P., and Sparrow, E. M., 1969, "Flow in the Hydrodynamic Entrance Region of Ducts of Arbitrary Section," ASME J. Heat Transfer, **91**(3), pp. 345–354.
[44] Schiller, L., 1923, "Uber den Stromungswiderstand von Rohrenverschiedenen Querschitts und Rauhigkeitsgrades," Z. Angew. Math. Mech., **3**, pp. 2–13.
[45] Nikuradse, J., 1930, "Untersuchungen uber turbulent Stromung in nicht kreisformigen Rohren," Ing. Arch., **1**, pp. 306–332.

Downloaded From: https://heattransfer.asmedigitalcollection.asme.org on 06/29/2019 Terms of Use: http://www.asme.org/about-asme/terms-of-use